Journal of Hazardous Materials 415 (2021) 125678

Contents lists available at ScienceDirect

Journal of Hazardous Materials

journal homepage: www.elsevier.com/locate/jhazmat

Research Paper

Stable mercury isotopes stored in Masson Pinus tree rings as atmospheric mercury archives

Xun Wang [a,b,*], Wei Yuan [a], Che-Jen Lin [c,d], Fei Wu [e], Xinbin Feng [a,f,*]

[a] State Key Laboratory of Environmental Geochemistry, Institute of Geochemistry, Chinese Academy of Sciences, Guiyang 550081, China
[b] College of Resources and Environment, Southwest University, Chongqing 400715, China
[c] Center for Advances in Water and Air Quality, Lamar University, Beaumont 77710, USA
[d] Department of Civil and Environmental Engineering, Lamar University, Beaumont 77710, USA
[e] Key Laboratory for Information System of Mountainous Area and Protection of Ecological Environment of Guizhou Province, Guizhou Normal University, Guiyang 550001, China
[f] Center for Excellence in Quaternary Science and Global Change, Chinese Academy of Sciences, Xian 710061, China

ARTICLE INFO

Editor: Dr. C. LingXin

Keywords:
Mercury isotopes
Tree rings
Radial translocation
Mercury pollution

ABSTRACT

The accuracy of mercury (Hg) dendrochemistry has been questioned because significant knowledge gaps exist in understanding the Hg translocation and mobility in tree-ring. In this study, we evaluated Hg concentrations and isotopic profiles in the tree-ring at a Hg artisanal mining site and a control site with the documented local Hg production inventory. Results show that the Hg concentration accumulated in tree-ring fails to reconstruct the temporal trend of Hg production due to confounded tree physiological and environmental factors, specifically, the radial translocation and tree age effects occurring during the fast-growing period. The temporal profiles of δ^{202}Hg exhibit pronounced tree-specific variabilities due to the complexity of Hg isotopic mass dependent fractionation during atmospheric Hg uptake and translocation in vegetation. The Hg odd-MIF (mass independent fractionation) profiles in tree-ring can reconstruct a decadal-scale temporal trend of the atmospheric Hg^0 pollution level, and also be used as a tracer to distinguish the emission source shifts of atmospheric Hg^0. However, the radial translocation would result in uncertainties at the higher resolution because of the mixing of odd-MIF signatures with active rings. Caution should be taken and additional supporting evidence collected from independent methods should be used for verifying the tree-ring records.

1. Introduction

The UN's Minamata Convention on Mercury has entered into force in August 2017 to protect environment and human health from the global mercury (Hg) pollution(UN-Environment, 2019). Understanding the response between Hg induced risk in the environment and long-term anthropogenic Hg emissions is the prerequisite for evaluating the impact of Minamata Convention. Monitoring of atmospheric Hg^0 concentration began only 20–30 years ago, and the absence of long-term measurements has limited assessment on atmospheric Hg pollution (Chellman et al., 2020; Clackett et al., 2018). The ability to infer the level of historical pollution using a readily available proxy offers opportunities to better understand the long-term and large-scale pollution of a global pollutant such as Hg. The Hg concentration records in natural archives, such as peat cores, ice cores, and sediment cores have been shown to be effective in reconstructing the historical atmospheric Hg pollution trends (Amos et al., 2013, 2015; Beal et al., 2015). Recently, tree ring has also been suggested as a promising proxy (Navratil et al., 2018; Peckham et al., 2019; Scanlon et al., 2020; Schneider et al., 2019), with advantages including the broad distribution of forests globally, easy and cost-effective sampling methods, accurate dating control in comparison to the radiometric chronology, centennial length chronologies, and simple pre-treatment for chemical analysis (Watmough, 1999).

Notwithstanding the advantages and demonstrated applications to reconstruct the centennial atmospheric Hg changes at local or regional scale (Chellman et al., 2020; Clackett et al., 2018, 2020; Ghotra et al., 2020; Kang et al., 2018; Navratil et al., 2018; Peckham et al., 2019; Scanlon et al., 2020; Schneider et al., 2019), the Hg dendrochemistry is still an emerging field of research (Arnold et al., 2018; Chellman et al.,

* Correspondence to: State Key Laboratory of Environmental Geochemistry, Institute of Geochemistry, Chinese Academy of Sciences, Lincheng Road 99, Guiyang, Guizhou, China.
E-mail addresses: wangxun@mail.gyig.ac.cn (X. Wang), fengxinbin@vip.skleg.cn (X. Feng).

https://doi.org/10.1016/j.jhazmat.2021.125678
Received 4 February 2021; Received in revised form 28 February 2021; Accepted 14 March 2021
Available online 19 March 2021

2020; Clackett et al., 2018; Peckham et al., 2019). Previous studies had mixed assessment on the suitability of using tree rings as archives for atmospheric Hg pollution trends. These studies have suggested pronounced variabilities within inter and intra tree rings (Clackett et al., 2018; Peckham et al., 2019), radial translocation of Hg between sapwood and heartwood (Arnold et al., 2018; Chellman et al., 2020; Peckham et al., 2019), tree age effects (young tree may be more sensitive to the atmospheric Hg change) (Peckham et al., 2019; Wright et al., 2014). The results indicate that tree rings are not a passive bio-monitor, and the observed Hg concentration trends are a result of complex physiological interactions between the vegetation and the environment. Other studies, however, have suggested that tree ring is a reliable proxy, with minimal to no influence from radial movement because the observed peak of Hg level in tree ring occurs during the time of high Hg emissions (Clackett et al., 2018; Kang et al., 2018; Navratil et al., 2018; Schneider et al., 2019).

The fundamental assumption of the Hg dendrochemistry is that Hg accumulated in tree ring is derived from the atmospheric Hg sources, and that there is a linear correlation between variations of Hg in air and in tree ring. Earlier studies using the controlled dose-response experiments (Arnold et al., 2018) and Hg isotopes (Wang et al., 2020b) have identified that Hg in tree ring is mainly from foliage uptake of gaseous elemental mercury (Hg^0) and subsequent translocation by the phloem. Given the relatively well documented Hg concentration in tree ring, an examination of the relationship between tree-ring Hg concentration and atmospheric pollution level is beneficial to using available data for determining historical Hg pollution.

We hypothesize that stable Hg isotopes stored in tree rings provide quantitative insight for understanding the pollution of atmospheric Hg^0. Mercury undergoes both mass dependent fractionation (MDF, represented by $\delta^{202}Hg$) and mass independent fractionation (MIF, as $\Delta^{199}Hg$, $\Delta^{200}Hg$ and $\Delta^{201}Hg$) during multiple processes occurring in forest ecosystems. Foliage uptake of atmospheric Hg^0 leads to a 2–3‰ MDF and lighter Hg isotopes accumulated in foliage (Wang et al., 2017, 2019, 2020a, 2020b; Yuan et al., 2020). The Hg odd-MIF signatures ($\Delta^{199}Hg$ and $\Delta^{201}Hg$) in foliage is mainly inherited from atmospheric Hg^0 (Wang et al., 2017, 2019, 2020a, 2020b; Yuan et al., 2020) but slightly modified by the Hg re-emission after the reductive loss from foliage (Yuan et al., 2019). Our recent work depicted that the MDF signatures in woody biomass vary among the tree components and species as a result of physiologically induced Hg accumulation and translocation, while the MIF does not occur because of little impact from physiological processes (Wang et al., 2020b). In addition, the odd-MIF signatures are useful tool to distinguish the Hg sources and transport in air since the atmospheric Hg^0 in remote regions is associated with distinct negative odd-MIF signatures (about −0.30‰ to −0.10‰) (Fu et al., 2016; Sun et al., 2019; Yu et al., 2016), but close to 0.00‰ when strongly influenced by anthropogenic Hg^0 emissions (Fu et al., 2019; Gratz et al., 2010; Yu et al., 2016). Therefore, an analysis on historical Hg emission inventories and potential changes of stable Hg isotopes yields a unique opportunity to examine using tree-ring data as a proxy for assessing the temporal trends of atmospheric Hg pollution level.

In this study, we determined centennial changes of Hg concentrations and the associated isotopic signatures in tree rings at a Hg artisanal mining site and a control site at Wanshan, Southwest China. To evaluate the effectiveness of using tree-ring data as the bioindicator for past atmospheric Hg^0 concentration, we compared the profiles of tree-ring Hg concentration and Hg isotopic signatures to the documented Hg production quantity at Wanshan from 1900 to 2018. We also examined potential biotic impacts to explain the discrepancies observed from the Hg concentration, isotopic records and Hg production data at Wanshan. Finally, implications on using Hg dendrochemistry for reconstructing atmospheric Hg^0 temporal trends are provided.

2. Materials and methods

2.1. Sites description

The studied sites are located at Wanshan, Guizhou Province, Southwestern China. Wanshan is known as the “Mercury Capital”, with the largest Hg deposit in China. The Hg mining activities have been documented for 3000 years in this area, and approximately 22,000 tons Hg, 15,920 tons of Ti_3Hg and $HgCl_2$ products, 6000 tons of cinnabar and large quantities of mine wastes were produced at Wanshan from 1900s to 1990s (Zhang et al., 2010). Wanshan has a humid sub-tropical climate with the annual mean value of 17 ℃. The annual precipitation is 1200–1400 mm, and 75% of total production occurs between April and October (Dai et al., 2012).

The information of selected two sites is shown in Fig. S1 of the Supportive Information (SI). One site is used for representing a Hg artisanal mining site, which is located at Gouxi (GX, 27.5625N, and 109.1909E) of Wanshan Hg mining area. The other is a control site at Guihuacun (GHC, 27.5336°N, and 109.3092°E), which is 12 km east of GX site. The GX site is about 5 km away from the Wanshan town, and 17 km to Tongren City, while the distance of GHC site to Wanshan and Tongren is 10–20 km farther. Although Hg mining activities in Wanshan have been ceased since 2003, the atmospheric Hg concentration at GX is still up to 211 ng m^{-3} in 2011, and 3–18 ng m^{-3} at GHC (Qin et al., 2020).

2.2. Sample collections and cross dating

We selected ten Masson pine trees at GX, including five trees with the breast-height diameter (BHD, 1.3 m height) of 90–120 cm, and five young trees with BHD of 30–50 cm to verify the tree age effects because the elevated atmospheric Hg^0 concentration at GX may lead to the tree age effects more clearly. At GHC, we selected 10 Masson pine trees with BHD of 90–120 cm. All selections were made in June 2019. Dual radii tree-ring cores of south-facing and west- or east- facing sides were collected at ~1 m height with a new 12-mm Haglöf increment borer and handled with nitrile gloves. The core samples were then sealed in the Teflon™ tubes with a diameter of 14-mm, and then washed by DDW (double distilled water) three times to remove potential dust, and dried in 50 ℃ oven for 5–7 days. Our earlier studies have suggested the oven drying at 50 ℃ does not lead to Hg loss from woody biomass (Wang et al., 2020b). After drying, 200- to 800-grit sandpapers were utilized to polish one side of the tree ring for observing individual rings. We followed a rigorous cross-dating of the tree-ring cores described by Sensula et al. (2017). The tree-ring widths were measured by a LINTAB 6.0 Pro (Germany) with a precision of 0.001 mm. The quality of the cross-dating was checked using the COFECHA program. The uncertainties of cross dating measurements do not significantly influence the tree-ring Hg records because of low resolution of Hg data (5- to 10-year resolution) and few absent or false rings in tree-ring cores of Masson pine.

2.3. Mercury concentration and isotopes measurements

After chronology development, we used a stainless-steel blade to dissect tree-ring core from one side of tree into 5-year growth increments for Hg concentration measurements. The other tree-ring core from the same tree is used to measure Hg isotopes. To remove potential surficial contamination after collection, we shaved the outer surface of tree-ring before Hg analysis. We used the Milestone tri-cell Direct Mercury Analyzer (DMA-80, Italy) to determine the Hg concentration. The quality assurance and quality control for woody Hg measurements has been described in our earlier studies (Wang et al., 2016, 2020b). Briefly, blanks and vegetation standard reference materials (GSB-27, Hg=12 ± 3 ng g^{-1}) were analyzed after every ten samples. The detection limit (0.01 ng Hg, n = 50 blanks) corresponds to a concentration of ~0.05–0.1 ng g^{-1} since all samples were wighted to ~0.1–0.2 g dry

wood. Standard reference materials yielded a recovery of 95–105%.

The Hg isotopes measurement needs 5–10 ng Hg mass in one sample. The warm and wet climate in the studied region leads to relatively fast growth of Masson pine, thus the 12-mm diameter annual rings can weight 20–80 mg wood mass. The Hg mass in 5-year growth increments at GX and in 10-year growth increments at GHC meets the 5–10 ng Hg need for Hg isotopes analysis beause of elevated Hg concentration in tree ring at the Hg mining site. The procedure for Hg isotope measurement of woody samples has been described elsewhere (Wang et al., 2020b) Briefly, all samples were processed by a double-stage tube furnace and trapping solutions (anti aqua regia) for Hg preconcentration. A modified dynamic temperature programming of the first combustion furnace was set as a 2.5 ℃ min^{-1} increase from 25 ℃ to 250 ℃ because the relatively low increase rate during the earlier oxidation stage of wood samples can constrain the Hg loss caused by the high level of gas formation. Then, we set 5–10 ℃ min^{-1} increase from 250 ℃ to 950 ℃. The second combustion furnace kept at 950 ℃ all-time (Fu et al., 2014). The Hg concentration enriched in 5-mL trapping solution (40% mixture of nitric and hydrochloric acid, HNO_3:HCl = 2:1, v/v) was then measured by a cold vapor atomic fluorescence spectrometry (Model 2500, Tekran® Instruments, Canada), and by following the US-EPA method 1631 (U.S. Environmental Protection Agency, 2002). Though we collected two-side tree-ring cores for the same tree, the DMA-80 measured Hg concentration in the tree ring of the other side cannot be utilized to calculate the recoveries of Hg preconcentration because of the variation of Hg concentration within a tree even for the same side of the trunk (Peckham et al., 2019). Given 95–103% recoveries of the standard reference materials (lichen standard reference, BCR-482, n = 6) during the procedure of Hg preconcentration, there is insignificant Hg loss in the tree-ring samples. The stable Hg isotope signatures of all samples were measured by multi-collector inductively coupled plasma mass spectrometer (MC-ICP-MS, Neptune II, Thermo Scientific, USA) at the State Key Laboratory of Environmental Geochemistry, Institute of Geochemistry, Chinese Academy of Sciences, following the standard-sample-standard (SPS) protocol and bracketing with a NIST SRM 3133 Hg solution as external standard-sample. The sample solution was diluted to 1 ng g^{-1} (10% acidity), which was then reduced by 3% $SnCl_2$ to Hg^0 in an online Hg vapor generation system. Instrumental mass bias correction was accomplished by using an internal Tl standard (NIST SRM 997). Tl standard was coupled into the plasma as aerosol particulate through a CETAC Ardius II desolvating nebulizer system.

The Hg-MDF is reported in δ notation using the unit of permil (‰) referenced to the neighboring NIST-3133 solution:

$$\delta^{202}Hg\ (‰) = 1000 \times [(^{202}Hg/^{198}Hg_{sample})/(^{202}Hg/^{198}Hg_{NISTSRM3133}) - 1] \quad (1)$$

MIF is reported as $\Delta^{xxx}Hg$ following the convention suggested by Blum and Bergquist (2007):

$$\Delta^{199}Hg\ (‰) = \delta^{199}Hg - 0.2520 \times \delta^{202}Hg \quad (2)$$

$$\Delta^{200}Hg\ (‰) = \delta^{200}Hg - 0.5024 \times \delta^{202}Hg \quad (3)$$

$$\Delta^{201}Hg\ (‰) = \delta^{201}Hg - 0.7520 \times \delta^{202}Hg \quad (4)$$

UM-Almadén secondary standard solution was analyzed for every 10 samples. Results of UM-Almadén ($\delta^{202}Hg$=−0.53 ± 0.04‰, $\Delta^{199}Hg$=−0.01 ± 0.04‰, $\Delta^{201}Hg$=0.01 ± 0.02‰, mean ± 1 standard deviation, n = 13) and BCR-482 ($\delta^{202}Hg$=−1.62 ± 0.06‰, $\Delta^{199}Hg$=−0.62 ± 0.05‰, $\Delta^{201}Hg$=−0.62 ± 0.04‰, mean ± 1 standard deviation, n = 6) are consistent with recommended values, and can be found in Table S1(Blum and Bergquist, 2007; Estrade et al., 2010).

2.4. Statistical methods

The data of Hg productions during 1899–2000 were obtained from the Wanshan Statistical Year Book. The Hg concentration in tree-ring shows insignificant correlations to core mass and raw ring-width data, consistent with earlier conclusion that the radial growth of the tree does not significantly dilute Hg concentrations (Clackett et al., 2018; Scanlon et al., 2020). Hence, the tree-ring Hg records do not require the same adaptive curve-fitting standardization procedures which is commonly used in the traditional tree-ring (paleo) environmental analysis. Linear regression analysis was performed to display the relationships among $\delta^{202}Hg$, $\Delta^{199}Hg$, $\Delta^{201}Hg$, and Hg concentration in tree-ring. Statistical tests, such as independent sample T-test and One-Way ANOVA at the 95% confidence were all preformed in SPSS Version 22.0. Because of the variabilities in tree-ring Hg data series, we did not use the arithmetic average value. Instead, the polynomial smooth spline was applied to obtain the average trend of tree-ring Hg series by the function of bs in R Language to reduce the noise of the data variabilities (more description and detailed code in Section S1 & S2 of SI). Earlier studies suggest a tree-specific bias adjusted method to deal with raw tree-ring Hg profile data(Clackett et al., 2018; Ghotra et al., 2020). The adjusted method does not significantly change the temporal trend of Hg concentration (Fig. S2; more description in Section S1 of SI), hence the temporal trends of raw data are reported.

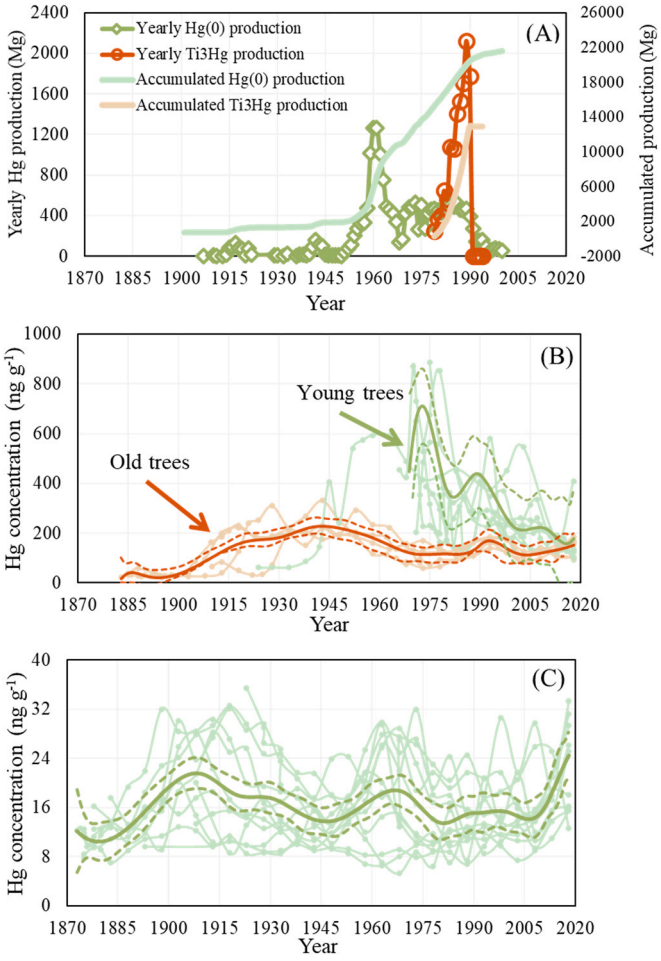

Fig. 1. (A) Hg production from 1899 to 2000 recorded in Wanshan Statistical Year Book; (B) Hg concentration trends in tree-ring sampled at GX; (C) Hg concentration trend in tree rings sampled at GHC. The bold solid lines in (B) and (C) represent polynomial smooth splines, and the dotted lines are the 95% confidence intervals for the simulation. It is noted that 1899–1905 with ~700 Mg production, but without detailed annual production data.

3. Results

3.1. Historic production and tree-ring concentration of Hg

Fig. 1A depicts the Hg production at Wanshan Hg mining regions from 1899 to 2000. The highest Hg^0 production peak occurs during 1953–1968 (8855 Mg). During 1970–1990, the Hg^0 production stays at the level of ~450 Mg yr^{-1}, then progressively decreases to 56.4 Mg yr^{-1} in 2000. There are three Hg^0 production peaks during 1939–1945 with a total of 502 Mg production, 1914–1922 with 550 Mg and 1899–1905 with ~700 Mg production (without detailed annual production data). In addition, the Ti_3Hg production starts from 1979 with an annual production of 245 Mg, then sharply increases to 1770–2120 Mg yr^{-1} during 1989–1990. The production ceased in 1991.

The tree-ring Hg series at GX exhibit high variability within intra-tree (Fig. 1B). The tree-ring Hg concentration at GX ranges from 21 to 2412 ng g^{-1} with average value of 263 ± 274 ng g^{-1} (median:186 ng g^{-1}). The tree-ring Hg records from young trees at GX (40- to 50-year-old) are significantly different from the matured trees (more than 100-year-old, Fig. 1B). First, the tree-ring Hg concentrations of young tree are 4–7 times higher than those of old tree during 1970–1985, and 1–4 time higher during 1985–2018. In addition, the tree-ring Hg temporal trends differ significantly between young and old trees. The young trees show peak Hg concentration (mean: 693 ± 72 ng g^{-1}) around 1975, then a continuous decrease with a rate of 35 ± 94 ng g^{-1} yr^{-1} during 1975–1985, and a second peak (mean: 438 ± 75 ng g^{-1}) around 1990. However, old trees do not show the peak around 1975, and only display a small peak around 1990 (170 ± 22 ng g^{-1}). In addition, the tree-ring Hg concentrations of old tree increase continuously from 1885 to 1940 at an average rate of 4 ± 2 ng g^{-1} yr^{-1}, then show a decrease trend with an average rate of 4 ± 2 ng g^{-1} yr^{-1} during 1940–1970.

The tree-ring Hg concentration at GHC also shows large variabilities among each core (Fig. 1C), in the range 5–35 ng g^{-1} with an average of 16 ± 6 ng g^{-1} (median:15 ng g^{-1}). From the 1870–1910 s, the average tree-ring Hg concentration at GHC increases from ~11 ± 2 ng g^{-1} to 22 ± 3 ng g^{-1}, and then decreases to 14 ± 2 ng g^{-1} in 1945. The average tree-ring Hg concentration at GHC increases with a rate of ~0.1 ± 0.1 ng g^{-1} yr^{-1} during 1945–1965, decreases with a rate of ~0.2 ± 0.1 ng g^{-1} yr^{-1} during 1965–1975, stays at an average of 15 ± 1 ng g^{-1} during 1975–2005, and then increases with a rate of ~1 ± 0.3 ng g^{-1} yr^{-1} to a final of 25 ± 2 ng g^{-1} in 2018.

3.2. Hg isotopic signatures in inter-tree and intra-stand

Given the variability among trees of difference ages (Fig. 2A and D),

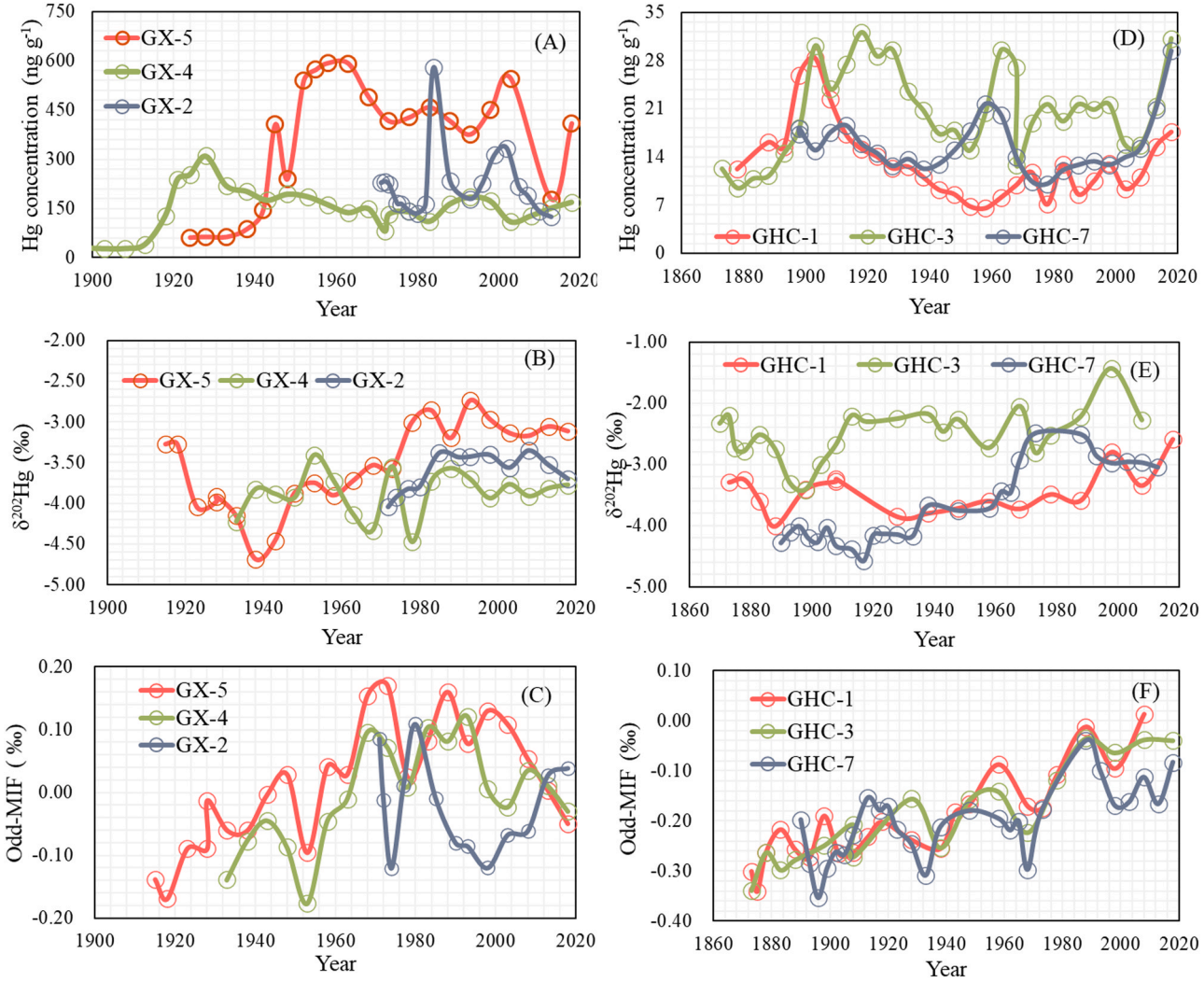

Fig. 2. (A)–(C) Trends of Hg concentration, Hg MDF ($\delta^{202}Hg$) and Hg odd-MIF ($\Delta^{199}Hg/2+\Delta^{201}Hg/2$) signatures in tree-ring at GX; (D)–(F) trends of Hg concentration, Hg MDF ($\delta^{202}Hg$) and Hg odd-MIF ($\Delta^{199}Hg/2+\Delta^{201}Hg/2$) signatures in tree-ring at GHC. The maximum SD (standard deviation) for $\delta^{202}Hg$ is 0.08‰, and for odd-MIF is 0.04‰.

we chose GX-2 (47-year), GX-5 (95-year) and GX-4 (130-year) at GX, and GHC-1(140-year), GHC-3 (145-year) and GHC-7 (120-year) at GHC for Hg isotopes analysis. The δ^{202}Hg at GX ranges from −5.06‰ to −2.53‰ with a mean value of −3.68‰ (median=−3.74‰, n = 58); Δ^{199}Hg is from −0.17–0.20‰ with a mean value of 0.01‰ (median=0.01‰, n = 58); and Δ^{200}Hg is from −0.06–0.09‰ with a mean value of 0.01‰ (median=0.01‰, n = 58). At GX (Fig. 2B), the δ^{202}Hg shows large variabilities temporally and among three tree-ring cores (all R^2 =0.00, $P > 0.05$). The δ^{202}Hg of GX-2 displays an increase trend (R^2 =0.462, $P < 0.05$) with an average rate of ~0.02‰ year^{-1} during 1970–2018. The δ^{202}Hg of GX-5 decreases from −3.27‰ in 1915 to −4.69‰ in 1938 (average of −0.058‰ year^{-1} rate), then increases to −3.11‰ in 2018 (average 0.019‰ year^{-1}, R^2 =0.713, $P < 0.05$). The δ^{202}Hg of GX-4 shows no temporal trend (R^2 =0.027, $P > 0.05$). The Δ^{199}Hg of GX-5 and GX-4 has a similar temporal trend (Fig. 2C), and the slope from the scatterplot of Δ^{199}Hg of GX-5 versus Δ^{199}Hg of GX-4 is 0.91 (R^2= 0.585, $P < 0.05$). Both GX-5 and GX-4 show three Δ^{199}Hg peaks around the 1910–1930 s, 1960s and 1980–1990s. The temporal trend of Δ^{199}Hg of GX-2 shows 5- to 10-year time lag compared to the trends of GX-5 and GX-4, which the peak occurring around 1980.

The δ^{202}Hg at GHC ranges from −1.44‰ to −4.74‰ with a mean value of −3.20‰ (median=−3.25‰, n = 69); Δ^{199}Hg is from −0.39 to 0.05‰ with an average value of −0.21‰ (median=−0.23‰, n = 69); and Δ^{200}Hg is from −0.10 to 0.09‰ with a mean value of 0.01‰ (median=0.00‰, n = 69). GHC-3 has the highest δ^{202}Hg (−2.50 ± 0.43‰ in GHC-3, −3.45 ± 0.37‰ in GHC-1 and −3.68 ± 0.67‰ in GHC-7, $P < 0.05$ by One-Way ANOVA test). In addition, the δ^{202}Hg of the three tree-ring cores displays large variabilities (Fig. 2E), and without significant correlations between each core ($P > 0.05$). The δ^{202}Hg of three tree-ring cores during 1890–2018 shows increasing trends, with an average of ~0.008‰ year^{-1} increase for GHC-1 (R^2 = 0.386, $P < 0.05$), an average of ~0.006‰ year^{-1} increase for GHC-3 (R^2 = 0.362, $P < 0.05$), and ~0.014‰ year^{-1} increase for GHC-7(R^2 = 0.732, $P < 0.05$). Different from δ^{202}Hg, the average values of Δ^{199}Hg among three tree-ring cores are comparable (−0.19 ± 0.09‰ in GHC-1, −0.19 ± 0.09‰ in GHC-3 and −0.21 ± 0.08‰ in GHC-7, $P > 0.05$ by One-Way ANOVA test). The Δ^{199}Hg values of three tree-cores at GHC exhibit consistent temporal trends, and show three peaks of Δ^{199}Hg in the year around the 1910–1930s, 1960s and 1980s (Fig. 2F). The three ring cores display an increasing trend of Δ^{199}Hg (R^2= 0.77 for GHC-1, 0.84 for GHC-3, and 0.49 for GHC-7; all $P < 0.05$, Fig. 2F) with a nearly 0.002‰ year^{-1} increase rate, i.e., from ~ −0.30‰ during the 1890 s to close 0‰ during the 2010s

Combining isotopic data of GX and GHC, the δ^{202}Hg data show a weak correlation with Δ^{199}Hg data (R^2 =0.01, $P > 0.05$) and the Hg concentrations (R^2 =0.04, $P > 0.05$), while Δ^{199}Hg values display a linear correlation with Δ^{201}Hg with slope of 1.0 (R^2 =0.872, $P < 0.01$), and a significant anticorrelation to the Hg concentrations (Figs. 3 and 4). Specifically, the higher Hg concentrations in tree-ring increments are associated with negligible of Δ^{199}Hg, while lower Hg concentration with negative Δ^{199}Hg (negative to −0.34‰, Δ^{199}Hg versus 1/Hg in Fig. 4.2).

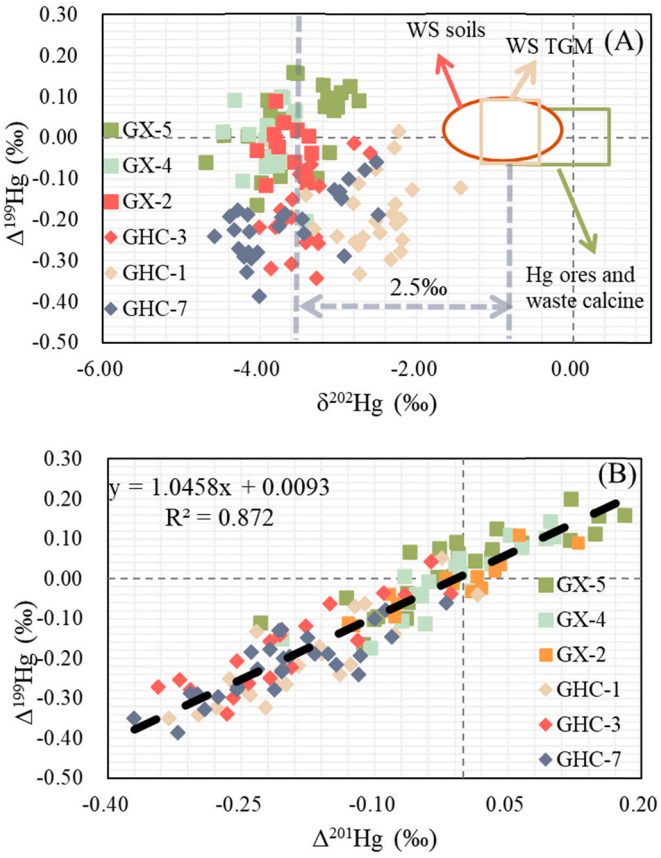

Fig. 3. (A) Variations of Hg MDF (δ^{202}Hg) and Hg odd-MIF (Δ^{199}Hg) signatures in tree ring; (B) Δ^{199}Hg signatures in tree-ring versus Δ^{201}Hg signatures in tree ring. The Hg isotopic signatures in WS (Wanshan) soils, WS Hg ore and waste calcine and present TGM are from the earlier studies(Qin et al., 2020; Yin et al., 2013). The maximum SD (standard deviation) for δ^{202}Hg is 0.08‰, and for odd-MIF is 0.04‰.

4. Discussion

4.1. Inconsistent Hg temporal series in tree rings

The extremely elevated atmospheric Hg^0 concentration at GX (Yuan et al., 2020) leads to 3 order of magnitude greater Hg concentrations in tree ring cores than in remote regions (usually 1–5 ng g^{-1}) (Chellman et al., 2020; Clackett et al., 2020; Ghotra et al., 2020; Peckham et al., 2019; Scanlon et al., 2020). The tree-ring Hg concentration at GHC is close to those observed near local anthropogenic sources in Europe (e.g., chlor-alkali plant and smelting sites) (Navratil et al., 2018, 2017). The elevated Hg concentration observed in tree rings at GX and GHC shows the impact of Hg mining activities on Hg accumulation in vegetation.

Several studies have indicated that the tree ring of coniferous species can be a reliable archive for atmospheric Hg^0 (Clackett et al., 2018, 2020; Ghotra et al., 2020; Peckham et al., 2019; Schneider et al., 2019). However, we found that the temporal profiles of Hg concentration in the tree-ring of Masson Pinus were inconsistent with the mining Hg production at Wanshan. During 1905–2000, there are four production peaks. Only the production peak of Ti_3Hg (~1990) corresponds to the Hg concentration peak at GX. Moreover, the Hg concentration in young tree-ring shows a decreasing trend during 1970–1985 at GX while the Hg production and concentration in the tree-ring of matured tree remains constant. At the GHC site, the 1960s′ peak is much smaller than the peak occurring in the 1910s while the Hg production during the 1960s is nearly 15 times than the production during the 1910s. These inconsistences between tree-ring Hg profiles and Hg production suggest the complexity of Hg uptake, translocation, and biological processes in vegetations that lead to Hg accumulation in tree rings.

The Hg concentration profile data both at GX and GHC exhibit pronounced tree-specific differences also observed in earlier studies (Chellman et al., 2020; Clackett et al., 2018, 2020; Navratil et al., 2018; Scanlon et al., 2020). The causes for the high variabilities of tree-ring Hg series are not well understood, but have been hypothesized to derive from several factors. One is tree physiological factors that influence foliage Hg uptake from the atmosphere and Hg translocation in phloem and xylem. These factors include but are not limited to the tree asymmetrical growth, stomata conductance, tree ages and canopy dynamics (Chellman et al., 2020; Clackett et al., 2018, 2020; Ghotra et al., 2020; Navratil et al., 2018; Peckham et al., 2019; Scanlon et al., 2020;

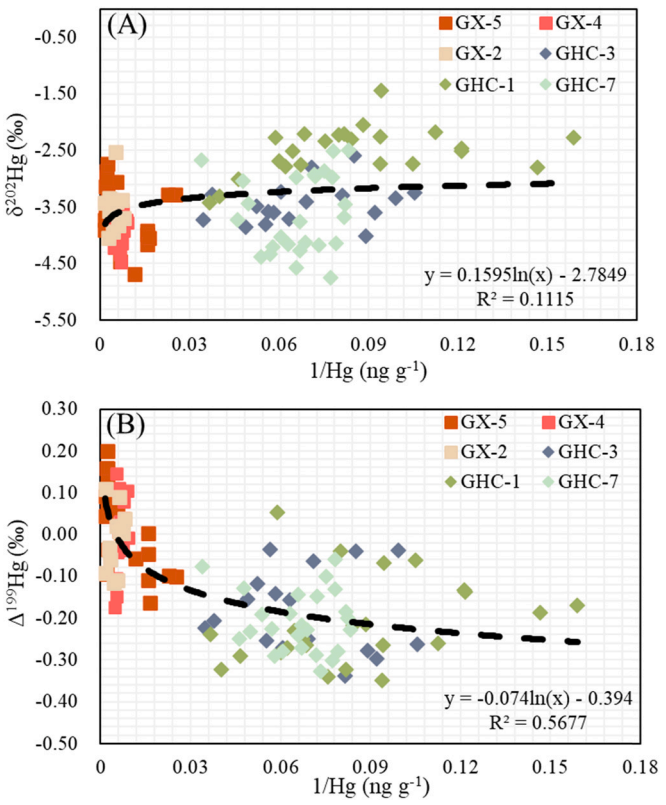

Fig. 4. (A) Variations of Hg MDF (δ^{202}Hg) signatures versus 1/Hg concentrations in tree ring; (B) Variations of Hg MIF (Δ^{199}Hg) signatures versus 1/Hg concentrations in tree ring.

Schneider et al., 2019). Another possibility is the environmental factors influencing the tree physiology, such as soil moisture, hill slope, wind direction, soil nutriments, etc. (Clackett et al., 2018; Ghotra et al., 2020; Scanlon et al., 2020). Among these factors, the possibility of radial translocation of Hg in xylem is currently under debate. Arnold et al. (2018) reported a radial translocation in active sapwood tree rings for 5-year-old Austrian pine, while Peckham et al. (2018) suggested no distinct evidence for lateral translocation between the tree rings for 6−7 year-old Pinus nigra. Later, the disparity between tree-ring Hg concentrations of young and old tree has been as attributed to the "tree age effects" that young trees have higher stomatal conductance and therefore greater Hg assimilation rates (Peckham et al., 2019). One study compared co-located ice-core and tree-ring Hg records (Chellman et al., 2020) and found generally paralleling between two archives with discrepancies in the timing and magnitude of elevated Hg events. An advection-diffusion model was constructed to explain these discrepancies caused by the radial translocation (Chellman et al., 2020). The understanding on the relationship of Hg variabilities and species-specific tree physiological response, while improving, is still limited because of a lack of direct evidences.

4.2. *Hg sources and translocation in tree rings revealed by Hg isotopes*

Few studies have reported Hg isotopic signatures of bole wood samples. The pitch pine at Shenandoah National Park, Virginia shows δ^{202}Hg ranging from −3.61‰ to −2.14‰, and −0.39‰ to −0.14‰ for Δ^{199}Hg (Scanlon et al., 2020); the spruce located at Mt. Gongga, China shows a mean δ^{202}Hg of −3.15 ± 0.22‰, and −0.14 ± 0.05 for Δ^{199}Hg (Wang et al., 2020b). These negative δ^{202}Hg and Δ^{199}Hg values in bole wood samples are similar to those observed in foliage(Scanlon et al., 2020; Wang et al., 2020b), indicating that the Hg in woods is mainly derived from the foliage uptake atmospheric Hg^0. In this study, the mean values of δ^{202}Hg in tree-ring are consistent with these earlier reported values (Table S2). The Δ^{199}Hg values of the present time (2010–2018) in all tree-ring samples are also similar to the Δ^{199}Hg signatures of atmospheric Hg^0 (Figs. 2C, F and 3A), consistent with the conclusion that Hg accumulated in woods comes from atmospheric Hg^0. All tree wood samples exhibit close to 0.00‰ signatures of Δ^{200}Hg(Scanlon et al., 2020; Wang et al., 2020b), suggesting that few Hg sources in woods are from direct atmospheric Hg^{2+} uptake.

Atmospheric Hg^0 isotopes undergo MDF during the foliage uptake, resulting in −2‰ to −3‰ shifts between δ^{202}Hg of atmospheric Hg^0 and foliage Hg (Demers et al., 2013; Wang et al., 2017). Average δ^{202}Hg of atmospheric Hg^0 in present time in Wanshan is −0.80 ± 0.63‰ (Qin et al., 2020). Comparing the average δ^{202}Hg values in tree ring to those of atmospheric Hg^0, an average of −2.5‰ shift (Fig. 3A) is found, similar to the reported shift during foliage Hg^0 uptake. It is likely that the negative δ^{202}Hg in tree ring comes from foliage δ^{202}Hg. However, the tree anatomy and physiology may also influence the MDF signatures in tree ring for several reasons. First, the δ^{202}Hg of tree ring has significant variabilities with intra-tree and intra-stand (Fig. 2B and E). Specifically, δ^{202}Hg of tree ring can be as low as −4.5‰, not seen in foliage (Table S2). Insignificant correlation between δ^{202}Hg and Hg production as well as between δ^{202}Hg and Hg concentrations (all $P > 0.05$) is found at Wanshan. This suggests that temporal shifts in Hg emissions during mining activities cannot solely explain the δ^{202}Hg variation in tree-ring (Figs. 1A and 4A). Moreover, the δ^{202}Hg generally displays a decreasing trend for first several decades from the bark to heartwood. We speculate that the potential radial translocation from sapwood to heartwood rings lead to the lighter Hg isotopes being accumulated in the tree ring toward heartwood. Finally, the δ^{202}Hg values show a negative correlation to ring width of GX-5 ($r = -0.51$, $P < 0.05$), GX-4 ($r = -0.471$, $P < 0.05$) and GHC-7 ($r = -0.58$, $P < 0.05$), but a weak correlation for other cores. These tree-specific correlations indicate the complexity of isotopic MDF induced from Hg uptake by foliage, downward translocation through the phloem to xylem, and subsequent radial translocation among sapwood and heartwood rings.

The processes causing ^{199}Hg MIF, magnetic isotope effect (MIE) and nuclear volume effect (NVE), do not occur during Hg translocation in vegetation (Wang et al., 2020b). The Δ^{199}Hg versus Δ^{201}Hg plot yields a slope of 1 (Fig. 3B), suggesting that photo-reduction before Hg translocation from foliage toward woods is the main cause for the odd-MIF. Different from the tree-specific variability of Hg concentration and δ^{202}Hg profiles (Fig. 2A, B, D and E), the Δ^{199}Hg profiles of GX-4 and GX-5 at GX, and GHC-1 and GHC-3 and GHC-7 at GHC show smaller differences within intra-tree (Fig. 2C and F). This indicates the physiological and environmental factors have limited influence on the Δ^{199}Hg variation in tree ring.

One possible cause to influence Δ^{199}Hg profiles is the different ratios of Hg sources mixing in each ring. Using a Δ^{199}Hg-Δ^{200}Hg triple-endmember mixing model, it has been found that nearly 84% of Hg in the stem of spruce at Mt. Gongga is derived from foliage Hg^0 uptake, and ~5% from atmospheric Hg^{2+} deposition and other geologic Hg sources (Wang et al., 2020b). Although the contribution of foliage Hg^0 uptake may vary in each ring, the relatively small contribution ratios of atmospheric Hg^{2+} deposition and geologic Hg sources do not lead to significant variation of Δ^{199}Hg. In this study, the observed Δ^{199}Hg at GHC before 1950 is smaller than −0.15‰, while the values in polluted soil are ~0.00‰ (Fig. 3A). This is consistent that the small variation of source fraction contributed by non-foliage derived Hg does not significantly influence the temporal trend of Δ^{199}Hg in tree-ring cores.

Since Δ^{199}Hg in tree ring is mainly derived from atmospheric Hg^0, the temporal shifts of Δ^{199}Hg signatures of atmospheric Hg^0 should result in the variations of Δ^{199}Hg in ring cores. This is supported by two observations. One is that the Δ^{199}Hg peaks occur during the 1910–1930s, 1960s and 1980–1990s (GX-5, GX-4, GHC-1, GHC-3 and GHC-7; Fig. 2C and F), coinciding with Hg peak productions at Wanshan. The nearly 0‰ Δ^{199}Hg in Hg ores and waste calcine (Fig. 3A) indicates

that higher Hg production leads to more positive Δ^{199}Hg shift in tree-ring profiles. This explains the more positive Δ^{199}Hg values during the high Hg production period. The Hg production peak during the 1960s is the highest, followed by the 1980–1990s, and then 1910–1930s (Fig. 1A). The highest shifts (up to +0.25‰) of Δ^{199}Hg occurred during the 1960s, +15–20‰ shifts during the 1980–1990s, and +5–10‰ shifts during the 1910–1930s both at GX and GHC. The shift of Δ^{199}Hg profiles can effectively track the relative changes of Hg emission strength.

The observed Δ^{199}Hg temporal variation can also be caused by radial translocation among sapwood and heartwood rings. Radial translocation potentially causes mixing of Δ^{199}Hg signatures with other active rings, leading to uncertainties in reflecting the trends of Δ^{199}Hg in air. Our data support the occurrence of radial translocation. One is the peak duration of Δ^{199}Hg is usually longer than the peak Hg production. For example, a Δ^{199}Hg peak duration of 1940–1970 was observed at GHC (Fig. 2F). However, the corresponding peak duration for Hg production is 1950–1970 (Fig. 1A). This means that the increasing trend of Δ^{199}Hg in tree-ring profile during 1940–1950 is likely caused by the positive Δ^{199}Hg of radial translocated Hg after 1950. The temporal trend of Δ^{199}Hg of GX-2 during 1970–2000 is similar with the trend of GX-4 and GX-5 during 1978–2008, indicating a 5- to 10-year time lag for GX-2 profile. The temporal trend of GX-2 is much more consistent with the GX-4 since 2000. We speculate that the period of 1970–2000 is the faster-growing time of GX-2. Therefore, the radial translocation occurs more readily because the wood grows actively. When the GX-2 reaches maturity (~30-year-old in 2000), the mobility of Hg among nearby tree-ring possibly decreases, and the Δ^{199}Hg profile is more temporally consistent with other matured trees.

4.3. Trends of atmospheric Hg isotopic signals revealed by tree rings

Comparison between Δ^{199}Hg profiles and Hg production shows that the Δ^{199}Hg profiles in tree-ring has potential to trace the shift of atmospheric Hg isotopes over decade time frame. The Δ^{199}Hg at GX is significantly more positive than values at GHC ($P < 0.05$, by independent T-test), consistent with the elevated Hg pollution at GX caused by Hg mining activities. The increasing trend of Δ^{199}Hg in GX-5 ($R^2 = 0.7236$, $P < 0.05$) and GX-4 ($R^2 = 0.7014$, $P < 0.05$) during the 1920–1970s at GX reflects the elevated Hg emission from the Hg mining processes and Hg mine wastes, with a gradual decrease of Δ^{199}Hg since 2000 s because the cease of Hg mining activities in Wanshan (Fig. 2C). After Hg production ceases, Hg emission from previously loaded Hg mining waste (Wang et al., 2007a, 2007b) contributes primarily to Hg pollution at GX (e.g., up to 211 ng m^{-3} in the year of 2011 (Qin et al., 2020)), leading to ~0‰ Δ^{199}Hg in ring cores at GX after the 2000s

At the controlling site GHC, the atmospheric Hg represents the mixture of the transported Hg from the mining regions, natural background Hg and local industrial Hg emission (Fig. 2F). The Δ^{199}Hg during the 1880s shows negative values (about −0.30‰), consistent with background foliage Δ^{199}Hg values across the globe (−0.31 ± 0.11‰) (Sun et al., 2019). Our earlier work has demonstrated that foliage Δ^{199}Hg is about 0.10‰ more negative than the Δ^{199}Hg of atmospheric Hg^0, which is caused by the processes of Hg re-emission from foliage (Yuan et al., 2019). We estimate that the Δ^{199}Hg of atmospheric Hg^0 is −0.20‰ during the 1880 s, consistent with the measured mean value of Δ^{199}Hg for background atmospheric Hg^0 (−0.11 ± 0.12‰, n = 220) (Sun et al., 2019). This indicates a small strength of Hg mining activities and anthropogenic emissions during the 1880s. With increasing Hg production and Hg mine wastes loading, an increasing Δ^{199}Hg profile in tree rings is evident until the end of 1980s. As discussed before, the peak values of Δ^{199}Hg during the 1910–1930s, 1960s and 1980s reflect the intensive Hg mining activities. Intriguingly, an increasing Δ^{199}Hg trend also occurs after the 2000s when the Hg mining ceased, suggesting additional atmospheric Hg sources at GHC. We speculate that the rapid urbanization at Wanshan and Tongren cities (20–30 km far away from GHC) since 2000s leads to a sudden increase of anthropogenic Hg emissions. The ~0.00‰ or slightly positive signatures of Δ^{199}Hg from anthropogenic Hg emissions (Blum et al., 2014; Sonke, 2011) drives the Δ^{199}Hg in tree-ring at GHC from −0.10 to −0.15‰ in 1995 to values of −0.04–0.05‰ in 2018.

4.4. Implications of tree-ring as an archive for atmospheric Hg and conclusions

In this study, the Hg concentration and Δ^{199}Hg do not exhibit a consistent temporal trend. The peak of Hg concentration during 1885–1930 at GHC is much higher than the peak during 1945–1975 (Fig. 1C). However, the Δ^{199}Hg values during 1885–1930 are 0.10–0.20‰ more negative (Fig. 2F), suggesting a less polluted level. This indicates that Hg concentration in ring cores is affected by multiple factors such as radial translocation and tree age effects. In addition, there are large inter-tree variabilities of Hg concentration profiles. Earlier studies have reported similarly high tree-specific differences among Hg concentrations, and suggest to reduce these uncertainties by increasing the tree-ring samples (e.g., tree numbers > 10), or using a tree-specific bias adjusted mean value to present the mean of all tree-ring Hg series (Clackett et al., 2018, 2020; Ghotra et al., 2020; Peckham et al., 2019). In Fig. S2B & S2C, adjusting (e.g., normalizing) tree-specific bias has no effect on the overall mean Hg concentration, but reduces the spread of data around the site-average record (Clackett et al., 2018; Scanlon et al., 2020). However, these statistical schemes do not rule out the possible influence of radial translocation and tree age effects, thus using Hg concentration profile in Masson Pinus tree rings to reflect the historical atmospheric Hg level still has substantial uncertainties.

Though few tree physiological processes induced Hg MIF signatures in tree ring, there are several limitations in using Δ^{199}Hg profiles to reconstruct the atmospheric Hg^0 concentration trends. First, the variation of Δ^{199}Hg may be not as sensitive as that of Hg concentration in tree-ring and the relation between Δ^{199}Hg and atmospheric Hg^0 concentration may not be linear, because the range of Δ^{199}Hg of atmospheric Hg^0 is relatively small at −0.30‰ to −0.10‰ for background air, and nearly 0.00‰ for polluted air (Blum et al., 2014; Sun et al., 2019). Second, Δ^{199}Hg approximately only reflects atmospheric Hg^0 pollution level and sources shifts at the decadal scale since the radial translocation can result in previously Hg isotopic signatures mixed with new signals at high resolution. Notably, the Hg concentration in tree-ring of background regions is low at 1–3 ng g^{-1}, and the 10-year increment of 12 mm ring core contains only ~1 ng Hg mass, insufficient for Hg isotopes measurements. We recommend mixing multiple tree-ring cores or at the resolution of several decades for background Hg isotopes measurements in tree-ring.

The Enrichment Factor (EF) estimates are calculated as the ratio of the modern to preindustrial Hg concentration, and widely used in natural archives to assess the impacts from strong anthropogenic Hg emissions since the industrial revolution. Currently, the EF estimated from tree-ring profiles is generally smaller than 2 (Chellman et al., 2020; Clackett et al., 2018, 2020; Ghotra et al., 2020; Kang et al., 2018), while the EF from other archives such as peat-core, ice-core and sediments usually ranges from 3 to 5 (Amos et al., 2013; Beal et al., 2015; Kang et al., 2016; Zdanowicz et al., 2016). This discrepancy can be explained by differences in preindustrial baseline period, by spatial variability in Hg deposition due to continentality, by seasonality of Hg^0 uptake in trees, and by non-atmospheric inputs from other archives (Chellman et al., 2020; Clackett et al., 2018, 2020; Ghotra et al., 2020; Kang et al., 2018). This study suggests that radial translocation and tree age effects during the fast-growing period can result in overestimated atmospheric Hg^0 pollution in first several decades of tree-ring growth, and thus a much smaller EF. Therefore, much caution should be paid in using tree-ring data as an archive to infer atmospheric Hg^0 pollution, especially in the absence of additional supporting evidence.

Finally, we conclude that the Hg odd-MIF profiles in tree-ring as a

better tracer than Hg concentration profiles to reconstruct a decadal-scale temporal trend of the atmospheric Hg^0 pollution level, and also can be used as a tracer to distinguish the emission source shifts of atmospheric Hg^0. Caution also should be taken when the tree-ring data are applied for constructing the history of atmospheric Hg because of the possible effect of the radial translocation. We recommend further works using co-located proxy comparisons of Hg isotopes and atmospheric Hg^0 dataset in global monitoring sites are needed to assess Hg uptake and its subsequent accumulation in tree rings is needed to gain better understanding.

CRediT authorship contribution statement

Xun Wang: Conceptualization, Formal analysis, Methodology, Visualization, Data curation, Writing - original draft, Writing - review & editing, Funding acquisition. **Wei Yuan:** Investigation, Resource, Methodology, Data curation. **Che-Jen Lin:** Writing - review & editing, Data curation. **Fei Wu:** Investigation and Resource. **Xinbin Feng:** Writing - review & editing, Funding acquisition.

Declaration of Competing Interest

The authors declare that they have no known competing financial interests or personal relationships that could have appeared to influence the work reported in this paper.

Acknowledgments

This work was funded by National Natural Science Foundation of China (41977272), Fundamental Research Funds for the Central Universities (SWU019037 and XDJK2020D041), Natural Science Foundation of Chongqing, China (cstc2020jcyj-msxmX006), National Natural Science Foundation of China (41829701 and 41921004) and K.C. Wong Education Foundation.

Appendix A. Supporting information

Supplementary data associated with this article can be found in the online version at doi:10.1016/j.jhazmat.2021.125678.

References

Amos, H.M., Jacob, D.J., Streets, D.G., Sunderland, E.M., 2013. Legacy impacts of all-time anthropogenic emissions on the global mercury cycle. Glob. Biogeochem. Cycl. 27, 410–421.
Amos, H.M., Sonke, J.E., Obrist, D., Robins, N., Hagan, N., Horowitz, H.M., Mason, R.P., Witt, M., Hedgecock, I.M., Corbitt, E.S., Sunderland, E.M., 2015. Observational and modeling constraints on global anthropogenic enrichment of mercury. Environ. Sci. Technol. 49, 4036–4047.
Arnold, J., Gustin, M.S., Weisberg, P.J., 2018. Evidence for nonstomatal uptake of Hg by aspen and translocation of Hg from foliage to tree rings in Austrian pine. Environ. Sci. Technol. 52, 1174–1182.
Beal, S.A., Osterberg, E.C., Zdanowicz, C.M., Fisher, D.A., 2015. Ice core perspective on mercury pollution during the past 600 years. Environ. Sci. Technol. 49, 7641–7647.
Blum, J.D., Bergquist, B.A., 2007. Reporting of variations in the natural isotopic composition of mercury. Anal. Bioanal. Chem. 388, 353–359.
Blum, J.D., Sherman, L.S., Johnson, M.W., 2014. Mercury isotopes in earth and environmental sciences. Annu. Rev. Earth Planet. Sci. 42, 249–269.
Chellman, N., Csank, A., Gustin, M.S., Arienzo, M.M., Vargas Estrada, M., McConnell, J. R., 2020. Comparison of co-located ice-core and tree-ring mercury records indicates potential radial translocation of mercury in whitebark pine. Sc. Total Environ. 743, 140695.
Clackett, S.P., Porter, T.J., Lehnherr, I., 2018. 400-year record of atmospheric mercury from tree-rings in Northwestern Canada. Environ. Sci. Technol. 52, 9625–9633.
Clackett, S.P., Porter, T.J., Lehnherr, I., 2021. The tree-ring mercury record of Klondike gold mining at Bear Creek, Central Yukon. Environ. Pollut. 268, 115777.
Dai, Z.H., Feng, X.B., Sommar, J., Li, P., Fu, X.W., 2012. Spatial distribution of mercury deposition fluxes in Wanshan Hg mining area, Guizhou province, China. Atmos. Chem. Phys. 12, 6207–6218.
Demers, J.D., Blum, J.D., Zak, D.R., 2013. Mercury isotopes in a forested ecosystem: implications for air-surface exchange dynamics and the global mercury cycle. Glob. Biogeochem. Cycl. 27, 222–238.
Estrade, N., Carignan, J., Sonke, J.E., Donard, O.F.X., 2010. Measuring Hg isotopes in bio-geo-environmental reference materials. Geostand. Geoanal. Res. 34, 79–93.
Fu, X., Marusczak, N., Wang, X., Gheusi, F., Sonke, J.E., 2016. Isotopic composition of gaseous elemental mercury in the free troposphere of the Pic du Midi observatory, France. Environ. Sci. Technol. 50, 5641–5650.
Fu, X., Zhang, H., Liu, C., Zhang, H., Lin, C.J., Feng, X., 2019. Significant seasonal variations in isotopic composition of atmospheric total gaseous mercury at forest sites in China caused by vegetation and mercury sources. Environ. Sci. Technol. 53, 13748–13756.
Fu, X.W., Heimburger, L.E., Sonke, J.E., 2014. Collection of atmospheric gaseous mercury for stable isotope analysis using iodine- and chlorine-impregnated activated carbon traps. J. Anal. At. Spectrom. 29, 841–852.
Ghotra, A., Lehnherr, I., Porter, T.J., Pisaric, M.F.J., 2020. Tree-ring inferred atmospheric mercury concentrations in the Mackenzie delta (NWT, Canada) peaked in the 1970s but are increasing once more. ACS Earth Space Chem. 4, 457–466.
Gratz, L.E., Keeler, G.J., Blum, J.D., Sherman, L.S., 2010. Isotopic composition and fractionation of mercury in great lakes precipitation and ambient air. Environ. Sci. Technol. 44, 7764–7770.
Kang, H.H., Liu, X.H., Guo, J.M., Xu, G.B., Wu, G.J., Zeng, X.M., Wang, B., Kang, S.C., 2018. Increased mercury pollution revealed by tree rings from the China's Tianshan mountains. Sci. Bull. 63, 1328–1331.
Kang, S., Huang, J., Wang, F., Zhang, Q., Zhang, Y., Li, C., Wang, L., Chen, P., Sharma, C. M., Li, Q., Sillanpaa, M., Hou, J., Xu, B., Guo, J., 2016. Atmospheric mercury depositional chronology reconstructed from lake sediments and ice core in the himalayas and Tibetan plateau. Environ. Sci. Technol. 50, 2859–2869.
Navratil, T., Simecek, M., Shanley, J.B., Rohovec, J., Hojdova, M., Houska, J., 2017. The history of mercury pollution near the Spolana chlor-alkali plant (Neratovice, Czech Republic) as recorded by Scots pine tree rings and other bioindicators. Sci. Total Environ. 586, 1182–1192.
Navratil, T., Novakova, T., Shanley, J.B., Rohovec, J., Matouskova, S., Vankova, M., Norton, S.A., 2018. Larch tree rings as a tool for reconstructing 20th century central European atmospheric mercury trends. Environ. Sci. Technol. 52, 11060–11068.
Peckham, M.A., Gustin, M.S., Weisberg, P.J., Weiss-Penzias, P., 2018. Results of a controlled field experiment to assess the use of tree tissue concentrations as bioindicators of air Hg. Biogeochemistry 142, 265–279.
Peckham, M.A., Gustin, M.S., Weisberg, P.J., 2019. Assessment of the suitability of tree rings as archives of global and regional atmospheric mercury pollution. Environ. Sci. Technol. 53, 3663–3671.
Qin, C., Du, B., Yin, R., Meng, B., Fu, X., Li, P., Zhang, L., Feng, X., 2020. Isotopic fractionation and source appointment of methylmercury and inorganic mercury in a paddy ecosystem. Environ. Sci. Technol. 54, 14334–14342.
Scanlon, T.M., Riscassi, A.L., Demers, J.D., Camper, T.D., Lee, T.R., Druckenbrod, D.L., 2020. Mercury accumulation in tree rings: observed trends in quantity and isotopic composition in Shenandoah national park, Virginia. J. Geophys. Res.: Biogeosci. 125, 125.
Schneider, L., Allen, K., Walker, M., Morgan, C., Haberle, S., 2019. Using tree rings to track atmospheric mercury pollution in Australia: the legacy of mining in Tasmania. Environ. Sci. Technol. 53, 5697–5706.
Sensula, B., Wilczynski, S., Monin, L., Allan, M., Pazdur, A., Fagel, N., 2017. Variations of tree ring width and chemical composition of wood of pine growing in the area nearby chemical factories. Geochronometria 44, 226–239.
Sonke, J.E., 2011. A global model of mass independent mercury stable isotope fractionation. Geochim. Cosmochim. Acta 75, 4577–4590.
Sun, R., Jiskra, M., Amos, H.M., Zhang, Y., Sunderland, E.M., Sonke, J.E., 2019. Modelling the mercury stable isotope distribution of earth surface reservoirs: implications for global Hg cycling. Geochim. Cosmochim. Acta 246, 156–173.
U.S. Environmental Protection Agency, 2002. Method 1631, Revision E: Mercury in Water by Oxidation, Purge and Trap, and Cold Vapor Atomic Fluorescence Spectrometry.
UN-Environment, 2019. Global Mercury Assessment 2018. UN-Environment Programme, Chemicals and Health Branch, Geneva, Switzerland.
Wang, S.F., Feng, X.B., Qiu, G.G., Shang, L.H., Li, P., Wei, Z.Q., 2007a. Mercury concentrations and air/soil fluxes in Wuchuan mercury mining district, Guizhou province, China. Atmos. Environ. 41, 5984–5993.
Wang, S.F., Feng, X.B., Qiu, G.L., Fu, X.W., Wei, Z.Q., 2007b. Characteristics of mercury exchange flux between soil and air in the heavily air-polluted area, Eastern Guizhou, China. Atmos. Environ. 41, 5584–5594.
Wang, X., Lin, C.-J., Lu, Z., Zhang, H., Zhang, Y., Feng, X., 2016. Enhanced accumulation and storage of mercury on subtropical evergreen forest floor: implications on mercury budget in global forest ecosystems. J. Geophys. Res.: Biogeosci. 121, 2096–2109.
Wang, X., Luo, J., Yin, R., Yuan, W., Lin, C.-J., Sommar, J., Feng, X., Wang, H., Lin, C., 2017. Using mercury isotopes to understand mercury accumulation in the montane forest floor of the Eastern Tibetan plateau. Environ. Sci. Technol. 51, 801–809.
Wang, X., Yuan, W., Lu, Z.Y., Lin, C.J., Yin, R.S., Li, F., Feng, X.B., 2019. Effects of precipitation on mercury accumulation on subtropical montane forest floor: implications on climate forcing. J. Geophys. Res.-Biogeosci. 124, 959–972.
Wang, X., Luo, J., Yuan, W., Lin, C.J., Wang, F., Liu, C., Wang, G., Feng, X., 2020a. Global warming accelerates uptake of atmospheric mercury in regions experiencing glacier retreat. Proc. Natl. Acad. Sci. U.S.A. 117, 2049–2055.
Wang, X., Yuan, W., Lin, C.J., Luo, J., Wang, F., Feng, X., Fu, X., Liu, C., 2020b. Underestimated sink of atmospheric mercury in a deglaciated forest chronosequence. Environ. Sci. Technol. 54, 8083–8093.
Watmough, S.A., 1999. Monitoring historical changes in soil and atmospheric trace metal levels by dendrochemical analysis. Environ. Pollut. 106, 391–403.

Wright, G., Woodward, C., Peri, L., Weisberg, P.J., Gustin, M.S., 2014. Application of tree rings [dendrochemistry] for detecting historical trends in air Hg concentrations across multiple scales. Biogeochemistry 120, 149–162.

Yin, R.S., Feng, X.B., Meng, B., 2013. Stable mercury isotope variation in rice plants (Oryza sativa L.) from the Wanshan mercury mining district, SW China. Environ. Sci. Technol. 47, 2238–2245.

Yu, B., Fu, X., Yin, R., Zhang, H., Wang, X., Lin, C.-J., Wu, C., Zhang, Y., He, N., Fu, P., 2016. Isotopic composition of atmospheric mercury in China: new evidence for sources and transformation processes in air and in vegetation. Environ. Sci. Technol. 50, 9262–9269.

Yuan, W., Sommar, J., Lin, C.-J., Wang, X., Li, K., Liu, Y., Zhang, H., Lu, Z., Wu, C., Feng, X., 2019. Stable isotope evidence shows re-emission of elemental mercury vapor occurring after reductive loss from foliage. Environ. Sci. Technol. 53, 651–660.

Yuan, W., Wang, X., Lin, C.J., Wu, C., Zhang, L., Wang, B., Sommar, J., Lu, Z., Feng, X., 2020. Stable mercury isotope transition during postdepositional decomposition of biomass in a forest ecosystem over five centuries. Environ. Sci. Technol. 54, 8739–8749.

Zdanowicz, C.M., Krummel, E.M., Poulain, A.J., Yumvihoze, E., Chen, J., Strok, M., Scheer, M., Hintelmann, H., 2016. Historical variations of mercury stable isotope ratios in Arctic glacier firn and ice cores. Glob. Biogeochem. Cycl. 30, 1324–1347.

Zhang, H., Feng, X.B., Larssen, T., Shang, L.H., Vogt, R.D., Lin, Y., Li, P., Zhang, H.I., 2010. Fractionation, distribution and transport of mercury in rivers and tributaries around Wanshan Hg mining district, Guizhou Province, Southwestern China: Part 2-Methylmercury. Appl. Geochem. 25, 642–649.